Molecular Dynamics of Human Methemoglobin: The Transmission of Conformational Information between Subunits in an $\alpha\beta$ Dimer

Nirmala Ramadas and Joseph M. Rifkind

Laboratory of Cellular and Molecular Biology, Molecular Dynamics Section, Gerontology Research Center, National Institute on Aging, National Institutes of Health, Baltimore, Maryland 21224 USA

ABSTRACT   Spectroscopic studies indicate an interaction of the distal histidine with the heme iron as well as the transmission of distal heme perturbations across the $\alpha_1\beta_1$ interface. Molecular dynamics simulations have been used to explain the molecular basis for these processes. Using a human methemoglobin $\alpha\beta$ dimer, it has been shown that at 235 K after 61 ps, a rearrangement occurs in the α-chain corresponding to the formation of a bond with the distal histidine. This transition does not take place in the β-chain during a 100-ps simulation and is reversed at 300 K. The absence of the distal histidine transition in the isolated chains and with the interface frozen indicate the involvement of the $\alpha\beta$ interface. A detailed analysis of the simulation has been performed in terms of RMS fluctuations, domain cross-correlation maps, the disruption of helix hydrogen bonds, as well changes in electrostatic interactions and dihedral angles. This analysis shows that the rearrangements in the α-chain necessary to bring the histidine closer to the iron involve alterations primarily in the CD loop and at the interface. Communication to the β-chain distal pocket is propagated by increased interactions of the α-chain B helix with the β-chain G-GH-H segment and the flexibility in the EF loop. The G helices shown to be involved in propagation of perturbation across the $\alpha_1\beta_1$ interface extend into the $\alpha_1\beta_2$ interfaces, providing a mechansim whereby distal interactions can modulate the T$\rightleftharpoons$R transition in hemoglobin.

INTRODUCTION

The desire to understand the cooperative binding of oxygen to hemoglobin has motivated much of hemoglobin research. The tertiary and quaternary structural changes caused by binding oxygen have been studied by comparing the static crystal structures of deoxyhemoglobin and oxyhemoglobin (Baldwin and Chothia, 1979; Fermi, 1975; Perutz, 1970; TenEyck and Arnone, 1976). On the basis of this comparison, major structural differences are observed during ligand binding. These include the movement of the iron into the heme plane, a change in the orientation of the proximal histidine, and rotation of the $\alpha\beta$ dimers relative to each other. These comparisons, supported by subsequent theoretical studies based on energy minimization, have defined an allosteric core (composed of the heme, part of the F-helix containing the proximal histidine, and the FG loop) that transmits conformational free energy from the heme pocket to the $\alpha_1\beta_2$ ($\alpha_2\beta_1$) interfaces, triggering a concerted cooperative transition from the unliganded T-state to the liganded R-state (Arata, 1995; Arata et al., 1988; Gelin et al., 1983).

The changes in the heme pocket emphasized by these studies are those on the proximal side of the heme. Changes are also found in the distal heme pocket when the x-ray structures of oxyhemoglobin and deoxyhemoglobin are compared. However, none of the proposed mechanisms satisfactorily link these distal changes with the binding of ligands and the major rearrangements at the $\alpha_1\beta_2$ interface. Therefore, the possible contribution of distal interactions to cooperativity has been neglected, even though the distal pocket plays an important role in regulating ligand affinity (Carlson et al., 1996; Perutz, 1989; Rifkind, 1988).

Thus it is well known from the static x-ray structure of hemoglobin and myoglobin that the ligand cannot gain access to the closed heme pocket. Structural fluctuations are necessary for the penetration of ligands from the solvent through the protein matrix to the closed heme pocket. These fluctuations involve large-amplitude correlated motions that require the concerted action of a large number of atomic degrees of freedom. Changes in these fluctuations can modulate the access to the heme pocket (Tsuruga et al., 1998) and the stability of the bound ligand (Tian et al., 1993), and may even play a role in cooperativity.

We have previously shown that in both Fe(II) and Fe(III) hemoglobin flexibility in the distal pocket can be monitored by following the low-temperature (210–250 K) interaction of the distal histidine with the heme iron (Levy and Rifkind, 1985; Levy et al., 1990, 1992). These interactions have been studied by Mossbauer spectroscopy for both Fe(II) and Fe(III) hemoglobin (Levy and Rifkind, 1985) and by electron paramagnetic resonance (EPR) for Fe(III) hemoglobin (Levy et al., 1990). It has also been shown that this flexibility increases for partially liganded Fe(II) hemoglobin (Levy et al., 1992). Changing the Fe(II) ligand of valency hybrids from O_2 to CO has been shown to produce a change in the distal pocket dynamic fluctuation of the Fe(III) subunits. By comparing different valency hybrids, it was further shown that these perturbations are transmitted across

the $\alpha_1\beta_1$ and $\alpha_2\beta_2$ interfaces (Levy et al., 1992). This finding was unexpected because negligible structural changes are found at these interfaces when the static crystal structures are compared.

In an attempt to understand the transmission from the ligand pocket across the $\alpha_1\beta_1$ and $\alpha_2\beta_2$ interfaces, it should first be noted that tertiary structural changes caused by the perturbation in the distal pocket have been shown to propagate as far as the B, G, and H helices located in the $\alpha_1\beta_1$ interface (Moffat et al., 1979). The absence of any noticeable crystallographic structural changes at the $\alpha_1\beta_1$ interface, even during the T-to-R transition, suggests that perturbations involving this interface are predominantly dynamic. Interestingly, the x-ray data on ligand binding in the T-state shows diffuse perturbations in this region, suggesting increased mobility (Anderson, 1973, 1975), that are greater than those observed in the $\alpha_1\beta_2$ interface. The $\alpha_1\beta_1$ interface contains more hydrophobic interactions than the $\alpha_1\beta_2$ interface and is disrupted only under extreme conditions (Atha and Riggs, 1976; Barksdale and Rosenberg, 1978; Kellett and Schachman, 1971; Rosemeyer and Huehns, 1967). Strong subunit interactions such as those involved in the $\alpha_1\beta_1$ interface are thought to require dynamic complementarity (Lumry and Gregory, 1989; Lumry, 1994), which would provide a mechanism where by alterations are readily transmitted across this interface.

These perturbations transmitted across the $\alpha_1\beta_1$ and $\alpha_2\beta_2$ interfaces may help to explain the recent studies that implicate more than two conformational states during hemoglobin oxygenation (Ackers et al., 1992; Bjorling et al., 1996; Bucci et al., 1993; Doyle and Ackers, 1992; Ho, 1992; Holt and Ackers, 1995; Huang and Ackers, 1995; Kwiatkowski et al., 1994; Perrella et al., 1992). Thus the rearrangements at the $\alpha_1\beta_2$ and $\alpha_2\beta_1$ interfaces associated with the T $\rightarrow$ R quaternary transition may still take place in a concerted manner. Intermediate states may, nevertheless, be associated with the transmission of dynamic perturbations across the $\alpha_1\beta_1$ and $\alpha_2\beta_2$ interfaces, which can modulate ligand affinity in either or both of the quaternary T and R states.

This paper provides the basis for explaining how perturbations are transmitted from the distal heme pocket across the $\alpha_1\beta_1$ and $\alpha_2\beta_2$ interfaces that undergo no major static structural changes, modulating dynamics in the heme pocket of another subunit. Differences in the response of the α- and β-chains to these distal heme perturbations are also discussed. Having established that the processes are dynamic in nature, we have used molecular dynamics simulations on an $\alpha\beta$ dimer of human methemoglobin. This dimer has been used because most of our studies directed at understanding perturbations and dynamics in the distal heme pocket are based on EPR studies using methemoglobin. The results on methemoglobin with a crystal structure similar to that of oxyhemoglobin are thought to be relevant to similar processes taking place in the functional Fe(II) hemoglobin. The detailed analysis was performed in terms of domain cross-correlation maps (DCCMs), individual he-

lical strengths, electrostatic interactions, and changes in dihedral angles.

METHODOLOGY

Molecular dynamics was carried out on methemoglobin, starting from the Perutz crystal structure deposited in the protein data bank (Ladner et al., 1977) and using the CHARMm version 22 force field (Brooks et al., 1983). Molecular dynamics simulations consisted of minimizing the starting structure to remove unrealistic van der Waals contacts by the adopted basis Newton-Raphson method, 2.35 ps heating to 235 K, 17.65 ps of equilibration, and 80 ps of production. The SHAKE algorithm (van Gunsteren and Berendsen, 1984) was used to remove the fastest vibrational motion involving hydrogens, thereby making the femtosecond time step meaningful.

The methods for efficient evaluation of long-range nonbonded interactions have been evolving continuously (Harvey, 1989; Lee and Warshel, 1992; Matthew, 1985; Sharp and Honig, 1990; Steinbach and Brooks, 1994), and various treatments of this interaction have been compared (Gained and Colman, 1993; Loncharich and Brooks, 1989; Mehler and Solmajer, 1991; Solmajer and Mehler, 1991; Stote et al., 1991). We have used optimum parameters to balance the accuracy of the simulation and economy of computer time. The nonbonded interactions were truncated at 12 Å, using a switching function starting from 8 Å, to smooth the energy function and to remove discontinuities in the force field at the point of truncation. The nonbonded list was calculated for pairs lying within 14 Å.

More than 5000 water molecules would be required to fully solvate the methemoglobin $\alpha\beta$ dimer. Molecular dynamics on such a solvated system would take an extremely long time, even on a supercomputer. One approach to modeling the polarizing effect of bulk solvent used in all of the simulations reported here is to screen the electrostatic interactions with a distance-dependent dielectric constant. This method also prevents unphysical grouping of charged groups at the finite cutoff distance of nonbonded interactions. In addition, only polar hydrogens were added to the globin, making the total number of atoms for the molecular dynamic simulations equal to 2827. By this procedure, it was possible to make comparisons between the isolated α-subunit, the isolated β-subunit, and the $\alpha\beta$ dimer under various conditions. These comparisons are essential to a discussion of the structural communication between the subunits and provide insights into the possible pathway by which it is achieved.

The residue PPX in the CHARMm PORPHYRINH.RTF file was modified by changing the charge of Fe to $+3$ and removing hydrogens on NB and ND. The charges on NB and ND were adjusted such that the new nitrogen charge was the sum of the prior nitrogen charge and that of the proton removed from it. Coordination bonds between the iron and the four nitrogens of the heme and the N_ϵ of the distal and proximal histidines are not defined. The iron nitrogen distances are therefore controlled by the van der Waal radii of the atoms and electrostatic interactions. The ligand water was treated as an independent group to be able to observe the motion of water either toward or away from the Fe.

The simulations were started with the crystal structure of one $\alpha\beta$ dimer of methemoglobin without any perturbation in the heme pocket, where the N_ϵ of the proximal histidine and the water are $\sim$2 Å from Fe. The N_ϵ of the distal histidine is at $\sim$4.7 Å from Fe. The adopted basis Newton-Raphson minimization followed by heating and equilibration results in a decrease in the distance between the N_ϵ of the proximal histidine and the Fe to 1.7 Å before the initiation of the molecular dynamics simulation. This distance, which is relatively short for an Fe nitrogen bond, is explained by the fact that these distances are driven mainly by nonbonded interactions. The electrostatic interactions between Fe^{3+} and the nitrogen result in a distance that approaches the van der Waal radii of these two atoms.

To show the importance of the $\alpha_1\beta_1$ interface in the coupling of tertiary and quaternary structural changes, molecular dynamic simulations were also performed on an isolated α-subunit, an isolated β-subunit, and a dimer with the interface frozen (no motion of residues in contact across the interface permitted). In an attempt to see the effect of temperature, molecular dynamics was also carried out on the starting structure at both 235 K and 300 K, keeping all other parameters the same.

RESULTS

Perturbations of the iron-ligand distances

To probe possible changes in the heme pocket configuration during the molecular dynamics simulations, we have analyzed (Fig. 1) the distance between iron and the oxygen of water and the distance between iron and the N_ϵ atom of both the distal histidine and the proximal histidine. Fig. 1 *a*
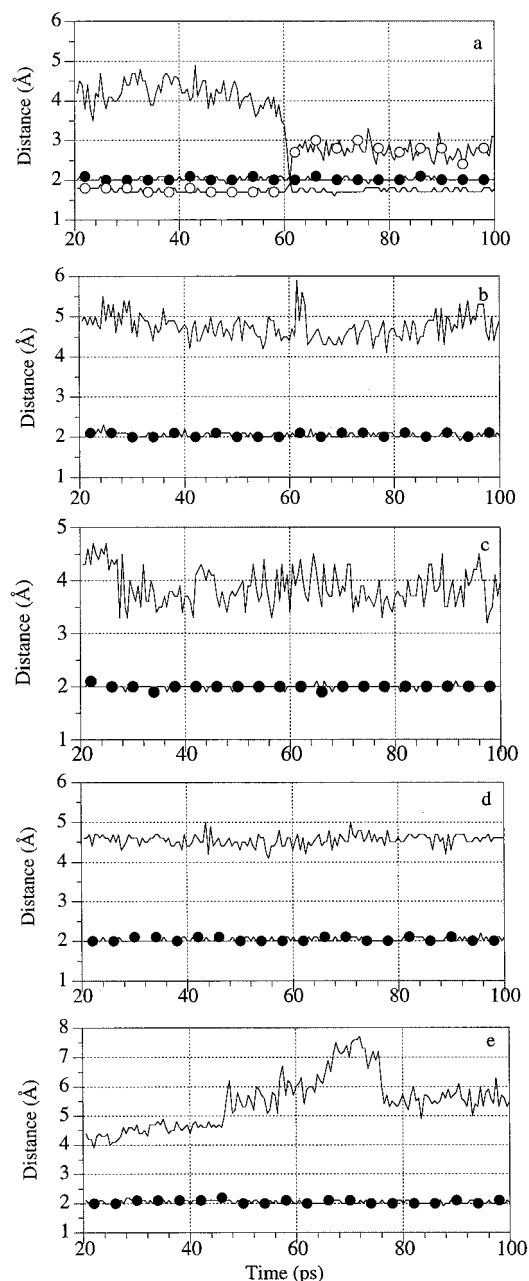

FIGURE 1   Changes in the distance of the ligands from the iron during 100-ps molecular dynamics simulations. Line with filled circles, O of water ligand; line without symbols, N_ϵ of distal histidine; line with open circles, N_ϵ of proximal histidine—only in *a*. (*a*) The α-chain in the simulation of an $\alpha\beta$ dimer at 235 K. (*b*) The α-chain in the simulation of an $\alpha\beta$ dimer at 300 K. (*c*) The simulation of an isolated α-subunit at 235 K. (*d*) The simulation of an isolated β-subunit at 235 K. (*e*) The α-chain in the simulation of an $\alpha\beta$ dimer at 235 K with the interface frozen.

shows the results on the α-chain of the $\alpha\beta$ dimer at 235 K. After 61 ps in the molecular dynamics simulation, there is a rearrangement in the coordination of the iron, with the distal histidine Fe-N_ϵ distance decreasing from 4.7 Å to 1.7 Å. At the same time, the Fe-N_ϵ distance of the proximal histidine increases from 1.7 Å to 2.5 Å. No change was observed in the Fe-O distance for water. These perturbations correspond to the binding of both water and the distal histidine to Fe on the distal side of the heme with a weakening of the proximal histidine bond. None of these changes are observed in the β-chain (data not shown). As shown in Fig. 1 *b*, these perturbations are not seen when the molecular dynamics simulation is performed at 300 K. These perturbations are also not seen even at 235 K with an isolated α-chain (Fig. 1 *c*) or an isolated β-chain (Fig. 1 *d*). In addition, they do not take place if the flexibility of the residues at the contact region of the two subunits is lost (Fig. 1 *e*). These results show that the transition at the α- heme (Fig. 1 *a*) is coupled to motion that takes place at the $\alpha\beta$ interface.

RMS fluctuations

RMS deviations from the average structure (B-factor) provide information about protein fluctuations. To understand the association between these fluctuations and the structural transition in the α-chain (Fig. 1 *a*), we have compared the RMS deviations before, during, and after the formation of the distal histidine-Fe bond (Fig. 2). In Fig. 2, *a* and *c*, only the backbone atoms were included, and in Fig. 2, *b* and *d*, all of the atoms (excluding hydrogen atoms) were included in the calculation.

In the α-subunit (Fig. 2, *a* and *b*), the fluctuation in the EF loop and parts of the F, G, and H helical segments, which has increased during bis-histidine formation, returns to its original value after the structural change. For the CD loop, the fluctuations increase during the transition and continue to increase even after the transition.

The possible involvement of β-chain residues in the α-chain transition and the effect of bis-histidine formation in the α-subunit on the β-subunit are shown by fluctuations for the β-subunit in Fig. 2, *c* and *d*. The regions near the AB and EF loops that showed relatively high flexibility in the 35–50-ps time range, before the α-chain bishistidine transition, undergo reduced fluctuations during and after the structural transition. A slight increase in the fluctuations of the G and H helices during the transition that subsides in the third time range is also detected. The involvement of the G and H helices can be explained by the intersubunit distance map (Fig. 3), which shows that these helices are in contact with α-chain residues at the interface. However, contacts at the interface do not directly explain the other changes in the β-subunit.

Domain cross-correlation map

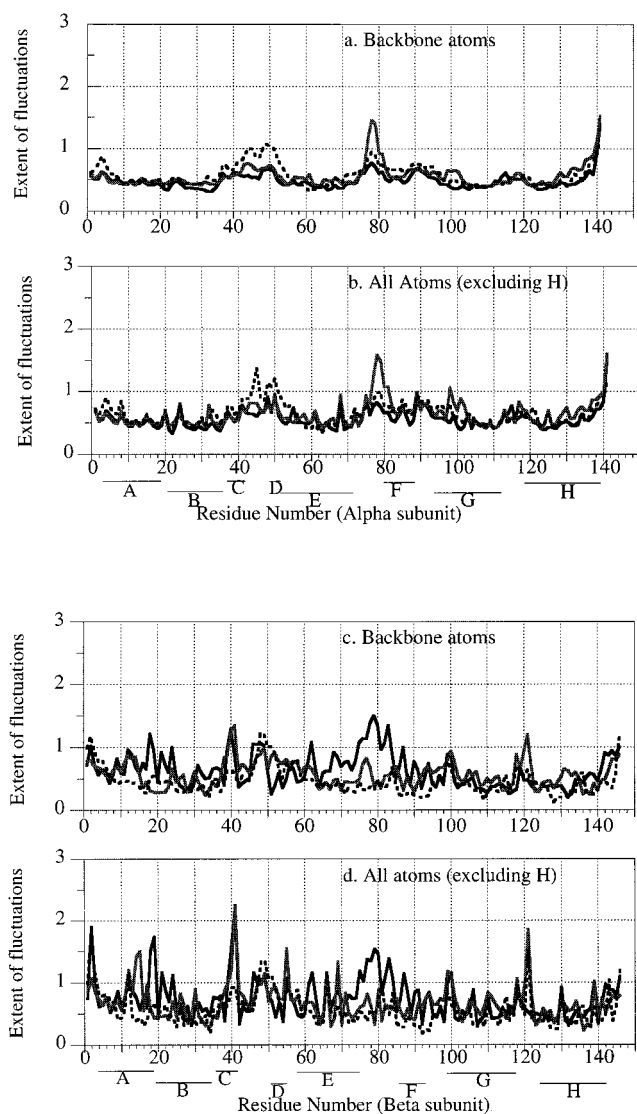The DCCM is a very powerful tool for viewing the concerted motion of various protein segments during dynamic

FIGURE 2   RMS fluctuations of residues in the α-subunit (*a* and *b*) and in the β-subunit (*c* and *d*) for different time ranges of the simulation. Solid line, 35–50 ps; gray line, 50–65 ps; dashed line, 65–80 ps.

fluctuations (Ichiye and Karplus, 1991), particularly when intersubunit coupled motions are involved (Komeiji et al., 1994; Swaminathan et al., 1991).

Fig. 4 shows the intrasubunit DCCM for backbone atoms of the α-subunit (Fig. 4, *A–C*) and the β-subunit (Fig. 4, *D–F*) in the three time ranges mentioned earlier (Fig. 2). The symmetrical intramolecular correlation matrix makes it possible to plot both positive and negative correlations in the same figure, with positive correlations plotted in the upper triangle and negative correlations plotted in the lower triangle. The regions that are either in contact or lying very close to each other will have a positive correlation, because they are not free to move independently. Long-range interactions, however, can produce either positive or negative correlations.

The intramolecular correlated motions in the α-subunit increase during the structural transition and further increase

after the transition (Fig. 4, *A–C*). A comparison of these figures reveals the important correlated motions associated with the structural transition. Of particular interest are the correlations that develop after the transition involving the E helix. The B, C, CD, and lower E regions became negatively correlated with the upper E and E-F region. The lower E region consists of Ser^{52} to Lys^{60} and contains the distal histidine (His^{58}). This dichotomy between the upper and lower E helix is also seen in the negative correlation of only the lower E helix with the H helix. Another noteworthy set of correlations is the positive correlation between the lower E and B helix as well as the B and G helix. These correlations are present, but weak, before the transition, intensify during the transition, and further intensify after the transition. There is also a pronounced increase in the positive correlation of the F and FG regions with the H helix after the transition.

These correlated motions provide insights into how perturbation involving the distal histidine in the E helix can be propagated to the interface. Fig. 4, *A–C*, actually suggests two pathways for the transmission of perturbations between the E-helix and the residues at the interface. One pathway involves transmission from the lower E helix to the B helix and then to the G helix in the interface. This pathway is already evident in the beginning of the simulation (Fig. 4 *A*) and is amplified during and after the transition. The second pathway involves the transmission across the heme to the F helix. From the F helix and FG loop these perturbations are then transmitted to the H helix in the interface, resulting in a negative correlation between the lower E helix and the H helix. Unlike the first pathway, this pathway is not evident until after the transition (Fig. 4 *C*), when the distal histidine already interacts with the iron (Fig. 1). It is this interaction that presumably weakens the proximal histidine iron bond (Fig. 1), causing a perturbation in the F helix, which is then propagated to the interface.

A comparison of Fig. 4, *A–C*, with Fig. 4, *D–F*, indicates that coupled motions linking the heme pocket and residues in the interface are different for the α and β residues. The coupled motions involving the first pathway described above are not initially seen (Fig. 4 *D*) in the β-chain and even after the transition (Fig. 4 *F*) are only poorly developed. The second pathway described above is observed, however, in the β-chain even initially (Fig. 4 *D*) and becomes very well developed after the transition (Fig. 4 *F*), even though the distal histidine has not moved closer to the iron. The observed correlated motion linking the E helix and the F helix without any changes in the iron coordination would probably not be propagated across the heme. Instead this pathway may be transmitted via the EF loop, which bridges the E and F helices. This loop shows unusually high fluctuations in the β-chain in the beginning of the simulation (Fig. 2, *c* and *d*), which may explain the correlated motion of the EF loop with the H helix in the earliest time frame (Fig. 4 *d*). The enhanced correlated motion in the β-chain after the transition in the α-chain indicates that the structural transition in the α-subunit perturbs the β-chain.
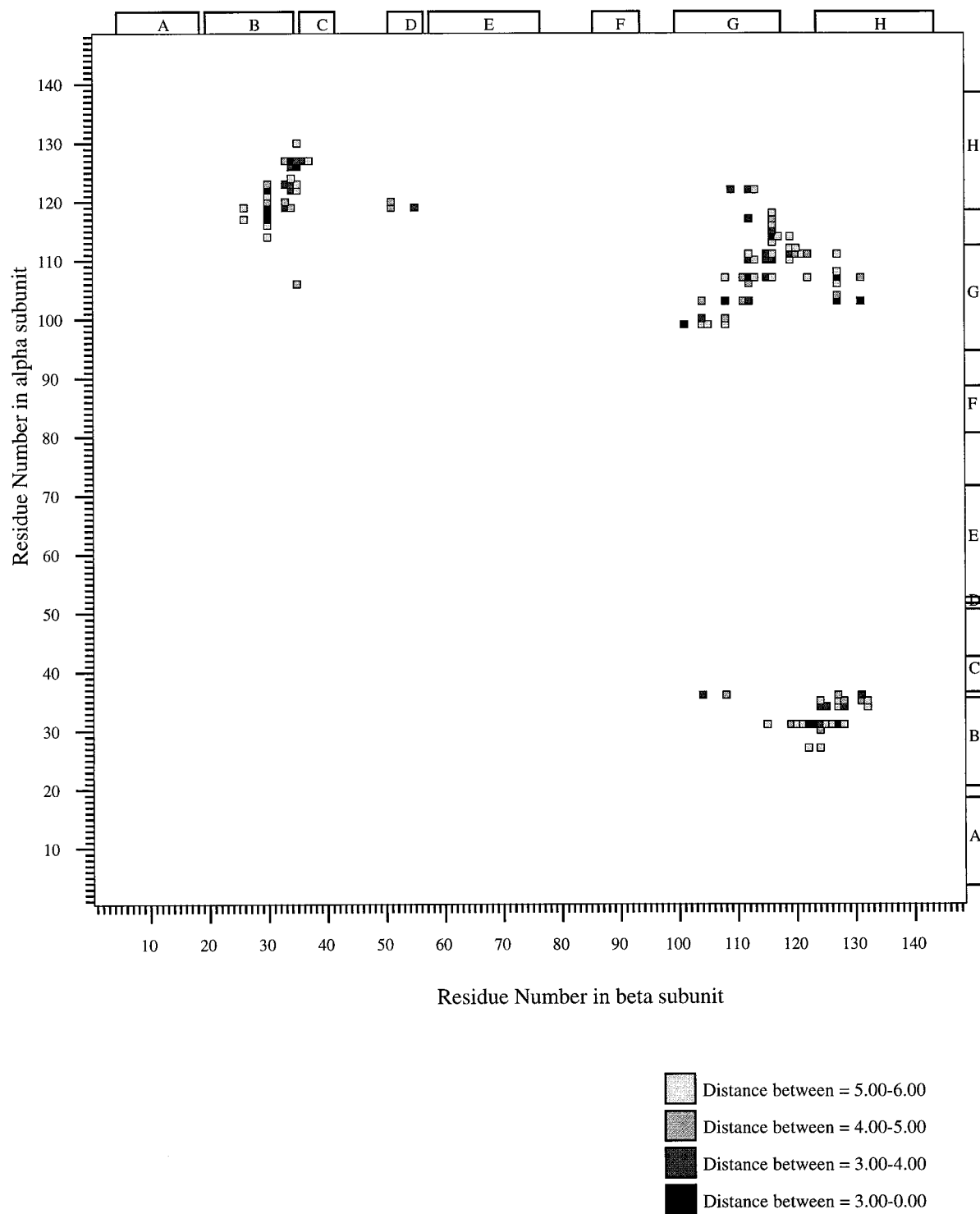
FIGURE 3   The intersubunit distance map of the $\alpha\beta$ dimer, indicating distances up to 6 Å.

The intersubunit correlated motions are shown in Fig. 5. The positive correlations before, during, and after the histidine transition in the $\alpha\beta$ dimer are shown in Fig. 5, A–C, and the negative correlations are shown in Fig. 5, D–F. From these intersubunit correlated motions, clear distinctions in the regions of contact between the α- and β-chains (Fig. 3) are discerned before, during, and after the 61-ps

transition in the α-chain (Fig. 5). In the pretransition 35–50-ps time frame, all of the contact regions show positive correlations, except for the contact involving G_α and H_β, for which motion is uncorrelated. During the transition, motion in this region becomes highly correlated. In the other regions of the interface, the dynamics of $(B-C)_\alpha$ and $(G-H)_\beta$ exhibit increased correlated motion, whereas the motion
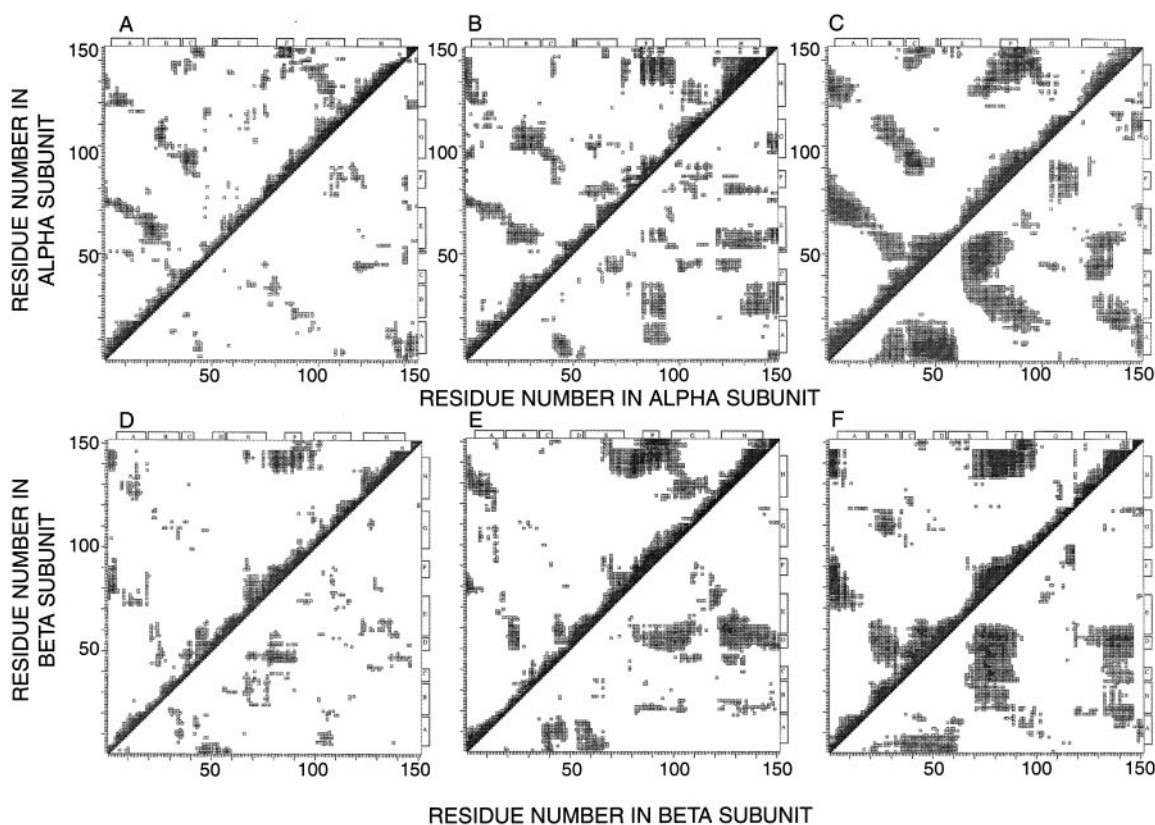
FIGURE 4 The intrasubunit DCCM for different time ranges of the $\alpha\beta$ dimer simulation. Positive correlations are shown in the upper left half of the plots, and negative correlations are shown in the lower right half of the plots. The magnitude of the correlation coefficients ranging from 1.00 (*solid black*) to 0.25–0.35 (*lightest gray*) is indicated by the intensity of the spots. (*A*) The α-subunit from 35 to 50 ps. (*B*) The α-subunit from 50 to 65 ps. (*C*) The α-subunit from 65 to 80 ps. (*D*) The β-subunit from 35 to 50 ps. (*E*) The β-subunit from 50 to 65 ps. (*F*) The β-subunit from 65 to 80 ps.

involving $(B-C)_\beta$ and $(G-H)_\alpha$ becomes less positively correlated. The positive correlated motions involving the G and H helices of both chains are further expanded after the transition to include a number of additional residues in the region. On the other hand, in the posttransition time frame the correlations involving $(B-C)_\alpha$ and $(G-H)_\beta$ are reduced back to their status before the transition. In conjunction with the growth and spreading of the positive correlated motions involving the G and H helices of both chains, an increase is also observed in negative correlated motions in the regions flanking this area of contact. These negative correlations, which increase from the first to the third time range, are H_α with (upper E-EF-F-FG)$_\beta$, H_β with H_α, (F-FG-G)$_\alpha$ with H_β, and (F-FG-G)$_\alpha$ with (upper E-EF-F-FG)$_\beta$. The extensive changes in correlated motions in the region of the interface is a clear indication of a perturbation in the region of the $\alpha\beta$ interface associated with the change in bonding at the α-heme.

Both negative and positive correlated motions that increase during and after the transition are also found in other areas, which are not directly in contact. These include negative correlations $(B-E)_\alpha$ with $(A)_\beta$, $(A)_\alpha$ with $(B-E)_\beta$, $(B-E)_\alpha$ with $(E-EF)_\beta$, (B-lower E)$_\beta$ with (upper E-EF)$_\alpha$, and positive correlations of (C-CD-lower E)$_\alpha$ with (C-CD-D-lower E)$_\beta$. Many of these correlations involve interactions

with the B, G, and H helices in the interface of one chain with segments from the other chain, which are not in the interface. These correlations thus indicate that motion across the interface is propagated to other parts of the dimer. Of particular interest, from our point of view, is the positive correlation between $(E-EF)_\alpha$ and $(E-EF)_\beta$ that indicates communication between the distal pockets of the two chains, even though these two regions of the dimer are ~40 Å apart. This communication can be rationalized in terms of the propagation of correlated motions within both the α-chain and the β-chain between the E-helix and the interface (Fig. 4, *C* and *F*).

Hydrogen bonds

The strength of a few of the hydrogen bonds stabilizing the helical segments is weakened during the simulation. This weakening is reflected in Fig. 6, where distances between the H of the -NH group of the ith residue and O of the carbonyl group of the $(i + 4)$th residue are plotted against time. The perturbation in these intrahelical hydrogen bonds reflects bending of the helical segment during the conformational perturbation. Loss of a hydrogen bond between His[58] and Val[62] at 61 ps is the result of the structural
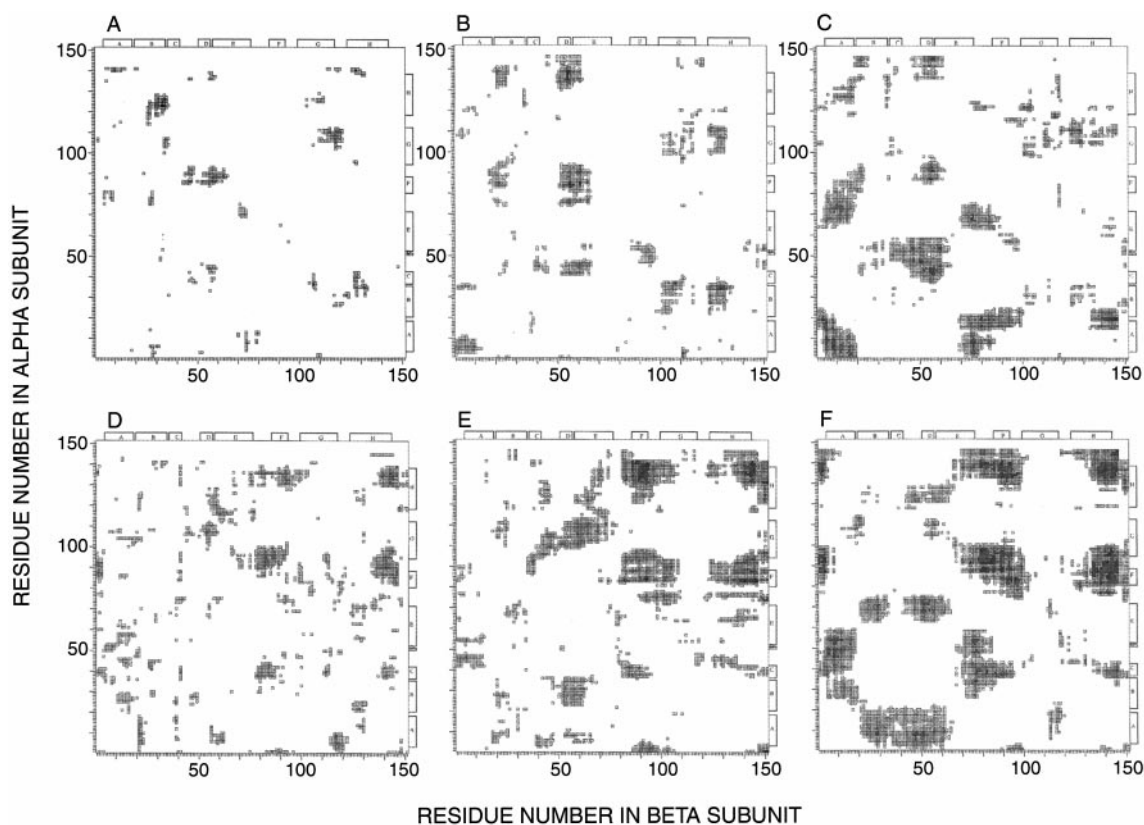
FIGURE 5   The intersubunit DCCM for different time ranges of $\alpha\beta$ dimer simulation. The magnitude of the correlation coefficients ranging from 1.00 (*solid black*) to 0.25–0.35 (*lightest gray*) is indicated by the intensity of the spots. (*A–C*) The positive correlations in the 35–50-ps, 50–65-ps, and 65–80-ps time ranges, respectively. (*D–F*) The negative correlations in the 35–50-ps, 50–65-ps, and 65–80-ps time ranges, respectively.

transition at 61 ps in the α-subunit. The breaking of the hydrogen bond of Lys[61] with Ala[65] at 55 ps in the E helix, Phe[98] with Ser[102] at 58 ps in the G helix, and Lys[99] with His[103] at 56 ps in the G helix may be involved in facilitating the structural rearrangement necessary for bonding of the distal histidine to the iron.

In the β-subunit, some of the hydrogen bonds are broken in the beginning of the trajectory itself (i.e., before 20 ps); however, the relevance of these bonds to the transition is not clear. The hydrogen bond between Asn[108] and Val[112] in the G helix, which breaks at 58 ps, supports the involvement of the $\alpha\beta$ interface in the transition.

Electrostatic interactions

Long-range nonbonded interactions are generally electrostatic in nature. To identify the electrostatic interactions involved in the structural transition at 61 ps, the electrostatic interactions of each residue were calculated with respect to the heme, the distal histidine, and the G helix for the entire trajectory.

Most of the energy leading to distal histidine-Fe bond formation is associated with an attractive force (Fig. 7) caused by the movement of the distal histidine closer to the Fe, which is only partially canceled out by the movement of the proximal histidine away from the Fe. The other electro-

static interactions (Fig. 7) are much weaker. However, because the bis-histidine bond cannot form by simply changing the orientation of the side chain of His[58], these electrostatic interactions may help drive the perturbations necessary for the bonding of the distal histidine to the heme iron. The small changes in the electrostatic interaction with the heme of the lower E helix residues E5, E10, and E11 at ~60 ps (Fig. 7) are consistent with a structural rearrangement involving the E helix. The weakening of the Fe bond with the N_ϵ of His[87] and the movement of the proximal histidine away from Fe cause changes on the proximal side of the heme. These perturbations are indicated by changes in the electrostatic interaction with the heme of His[87] and other F helix residues (F3, F4, F7, and F9). Some of the F helix residues (i.e., Leu[83] and Leu[86]) show changes in the electrostatic energy that begin at ~60 ps but continue for some time. These changes are suggestive of perturbations being propagated through the molecule.

Interestingly, residues 94–102 of the G helix also show significant change in the electrostatic energy with the heme around 60 ps, indicating that the conformational changes in the heme pocket are also associated with the interface. Similar changes in electrostatic energy found between the α-chain heme and the β-chain G helix residues Arg[104] and Asn[108] (data not shown) indicate that the conformational change in the heme pocket of one subunit is felt in the other
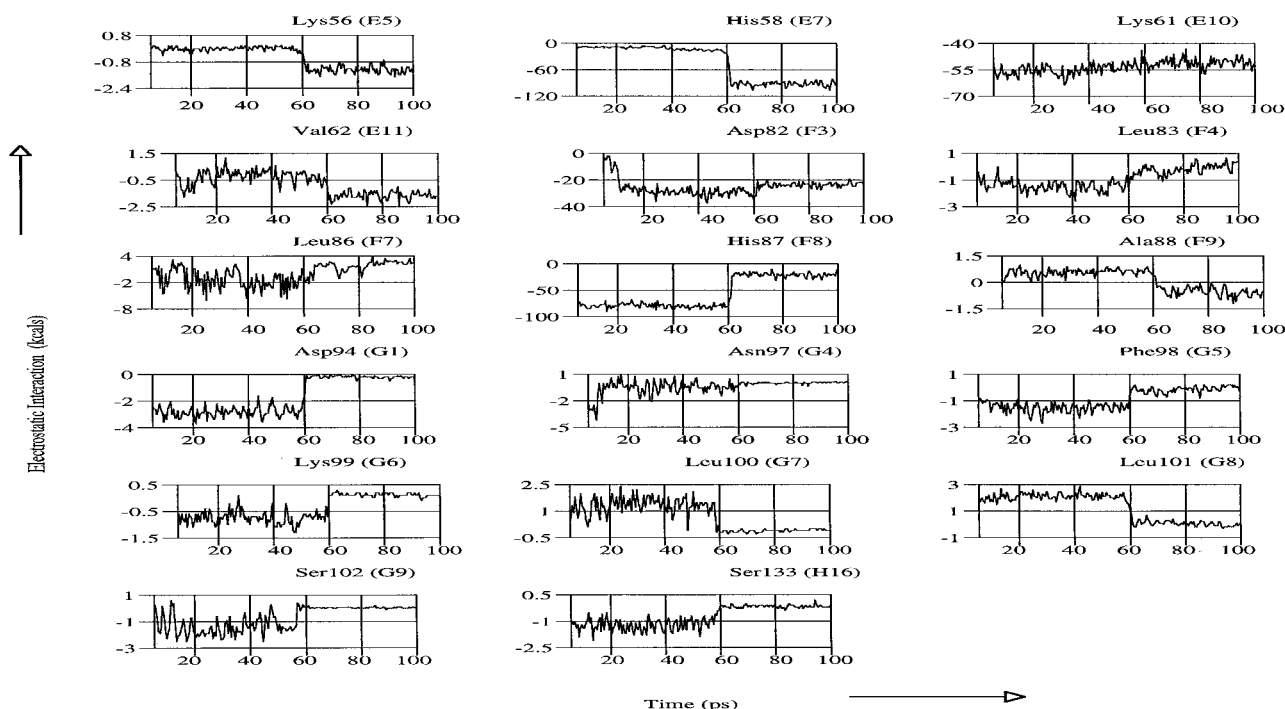
FIGURE 6   The integrity of the helix hydrogen bonds for the helical segments as indicated by carbonyl O(i) to amide H($i + 4$) distances in the range of 1.50–2.00 Å (*black*) and 2.00–2.50 Å (*gray*). (*a*) In the α-subunit. (*b*) In the β-subunit.

subunit through the interface. These changes in the electrostatic energy between the heme and the G helix residues may actually be associated with the hydrogen bonds that are broken in the G helices of both chains (Fig. 6). The broken hydrogen bonds facilitate changes in the nonbonded heme distances, resulting in altered electrostatic energy.

To further investigate the involvement of the G helix in the α-subunit transition, electrostatic interactions of the residues of the α-chain G helix with other groups (data not shown) were studied. As expected, the interaction between residues 94–102 of the G helix with the water ligand, the proximal histidine (His[87]), and the distal histidine (His[58]) in the α-subunit show changes at the time of bis-histidine bond formation.

Dihedral angles

The dihedral angles that define the configuration of each amino acid are perhaps the most sensitive measure of local structural alterations. It is, therefore, perhaps the best way to gain insight into the changes occurring during the initial 60 ps of the trajectory, which facilitate bis-histidine bond formation.

We have investigated the changes in the dihedral angles for each residue within 5 Å of the distal histidine during the 100-ps molecular dynamics simulation. The dihedral changes observed can be divided in to three classes: 1) the changes occurring before 60 ps, which may be responsible for the bis-histidine bond formation by influencing the orientation and position of His[58]; 2) the changes occurring

at 60 ps, which may still assist bis-histidine bond formation by accommodating the changes in His[58]; and 3) the changes that occur after 60 ps, which arise as a result of bis-histidine bond formation. Of these, we have focused primarily on the first class of dihedral angle changes to gain insight into the formation of the iron distal histidine bond. Residues that undergo changes before 60 ps (Fig. 8) are found in the CD loop (Asp[47], Leu[48], His[50]), in the E helix (Gln[54], Leu[68]), in the G helix (Asn[97], Phe[98], Lys[99]), and in the H helix (Thr[134]). The residues Leu[106] (G8), Arg[116] (G18), Lys[120] (GH3), and Glu[125] (GH8) in the β-subunit, which are within 5 Å of the α-chain distal histidine (His[58]), also show dihedral changes before 60 ps. The multiplicity of changes involving the G and H helices (particularly the G helix) indicates the importance of the B-G-H framework of the $\alpha_1\beta_1$ interface in facilitating the formation of the bis-histidine complex. The resides belonging to the second category of dihedral changes (data not shown), which may stabilize the transition, are Lys[61] (E10), Val[62] (E11), and Asp[75] (EF4).

DISCUSSION

Coordination of the distal histidine with the iron

Molecular dynamics simulation at 235 K on a methemoglobin $\alpha\beta$ dimer for 100 ps shows the spontaneous formation of a bis-histidine complex in the α-chain at 61 ps without the formation of any bis-histidine complex in the β-chain. An analogous heme pocket configuration for oxyhemoglo-
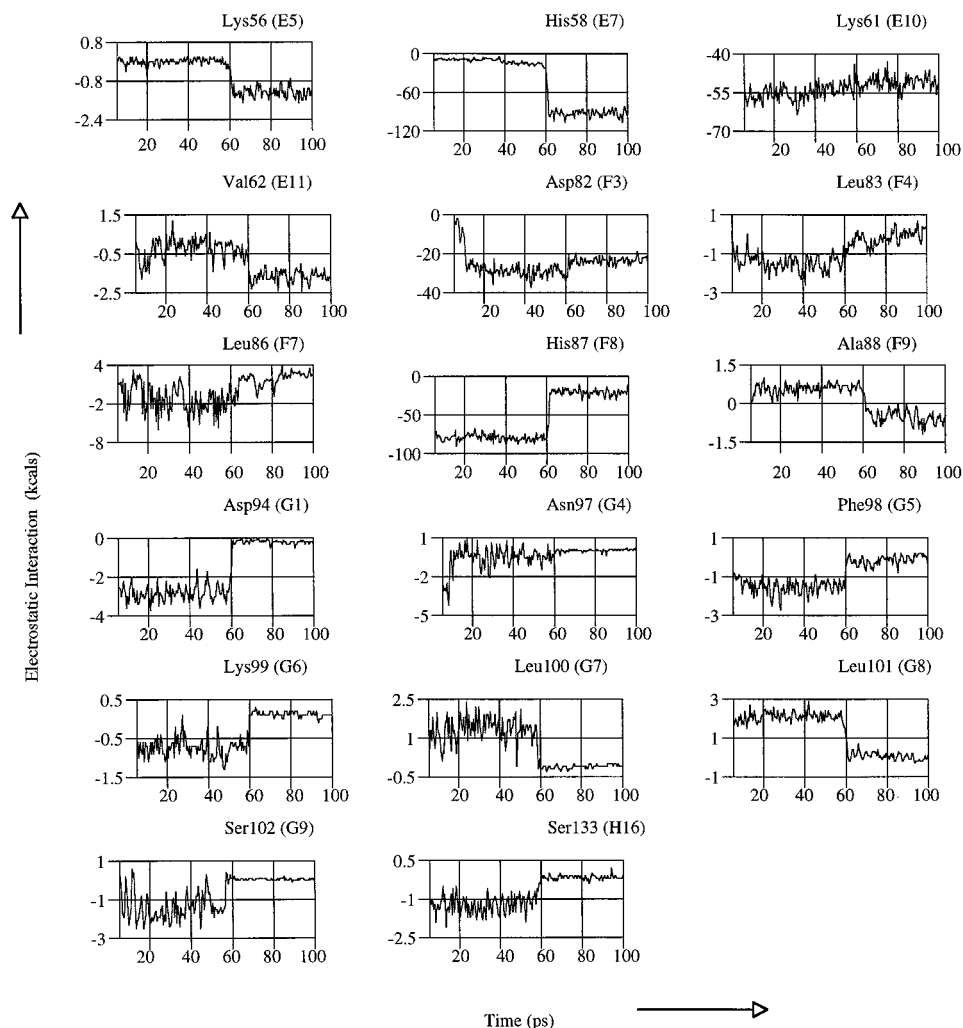
FIGURE 7 The changes in the electrostatic energy between the α-chain heme group and various residues (as marked) during the 100-ps simulation.

bin whereby the distal histidine approaches the iron has been postulated to explain autoxidation of hemoglobin (Balagopalakrishna et al., 1996). In this mechanism the distal histidine acts as an endogenous nucleophile to displace the bound oxygen as a superoxide. In this respect it is interesting that the β-chain, which does not form a bond between the iron and the distal histidine in our simulation, undergoes much slower autoxidation (Tsuruga et al., 1998) than the α-chain, which does form this bond.

This α-chain transition does not happen if the simulation is carried out at 300 K. Furthermore, if the distal histidine is brought closer (1.7 Å) to Fe, using distance constraints, and molecular dynamics is then performed on the resultant structure at 300 K, the distal histidine moves away from Fe at ~67 ps (Nirmala and Rifkind, unpublished results). These observations suggest a temperature-dependent shift in the equilibrium between methemoglobin with water coordinated to Fe and a configuration with both the distal histidine and water within bonding distance of the heme Fe.

We have previously shown, by electron paramagnetic resonance (EPR) studies, that a configuration similar to that produced during the simulation with both histidine and

water in close proximity to heme Fe (Levy et al., 1990) is produced during incubation at 235 K. Rapid freezing of an ambient-temperature methemoglobin sample further indicates that low levels of this configuration are present even at room temperature. Based on these studies, a rapid equilibrium was proposed to exist between the usual methemoglobin state with water bound to iron in the sixth coordination site and a seven coordinated state with both the water and the distal histidine coordinated with the heme. Such a rapid equilibrium is supported by the 61-ps structural transition observed in the present molecular dynamics simulation.

The shift in equilibrium toward the distal histidine coordinated state seen in our molecular dynamics simulations at 235 K has also been found in the EPR studies on methemoglobin (Levy et al., 1990), as well as in Mossbauer studies on both methemoglobin and deoxyhemoglobin (Levy and Rifkind, 1985). In those studies it was shown that decreasing the temperature from 300 K to a temperature in the range of 210–250 K increases the population of species with the distal histidine coordinated to iron. It has been suggested that the driving force for the coordination of the distal histidine to the iron is the stability of the Fe-distal
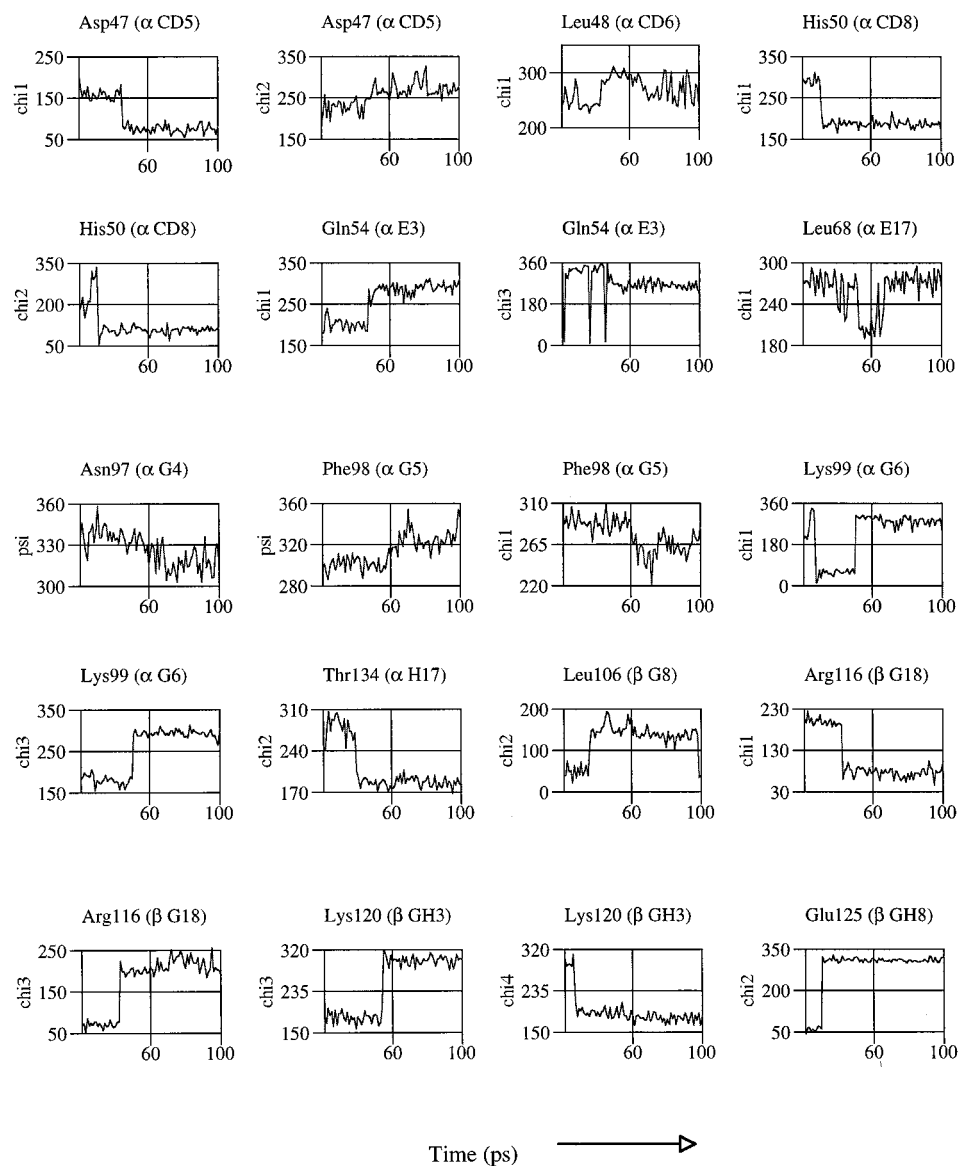
FIGURE 8   The changes in specified dihedral angles of selected residues during the 100-ps simulation.

Time (ps) ——————▷

histidine bond. At 300 K minimal bond formation occurs because of the greater configurational entropy, which cannot be compensated for by bond formation.

The bonding of the distal histidine to the Fe requires a 2–3-Å movement of the distal histidine N_ϵ. This movement is not possible by simple rotation of the distal histidine imidazole ring and requires a rearrangement of the globin on the distal side of the heme. This rearrangement is shown in Fig. 9, which compares the distal side of the heme from the CD loop to the EF loop of the α-chain in the initial methemoglobin structure with a snapshot of the 70-ps structure after the distal histidine bond has formed. The molecular rearrangement required for the formation of a bis-histidine complex is the basis for relating the low-temperature formation of this complex with flexibility in the distal heme pocket (Levy and Rifkind, 1985). In oxyhemoglobin it has been proposed that the lower rate of autoxidation in the β-chain is due to constraints on the movement of

the distal histidine (Tsuruga et al., 1998), i.e., to decreased flexibility. Detailed insights into the factors that control the distal heme pocket configuration, however, are very difficult to obtain experimentally and can therefore be most readily obtained by molecular dynamics simulations.

Involvement of the αβ Interface

Involvement of the αβ interface in forming the distal histidine bond is demonstrated (Fig. 1) by molecular dynamics simulations under identical conditions on an isolated α-subunit, an isolated β-subunit, and an αβ dimer with the interface frozen (i.e., no motion was permitted for the residues at the interface), which fail to show any bis-histidine bond formation. The role of the interface is confirmed by the H-bonds broken in the G helix (Fig. 6), the changes in electrostatic interactions involving residues in the G helix

FIGURE 9   Comparison of the initial structure (*red*) of the α-chain with the structure (*yellow*) after formation of the distal histidine bond (depicted by the 70-ps snapshot). Shown are the iron, the proximal histidine, and the globin on the distal side of the heme from residue 43 to residue 77.
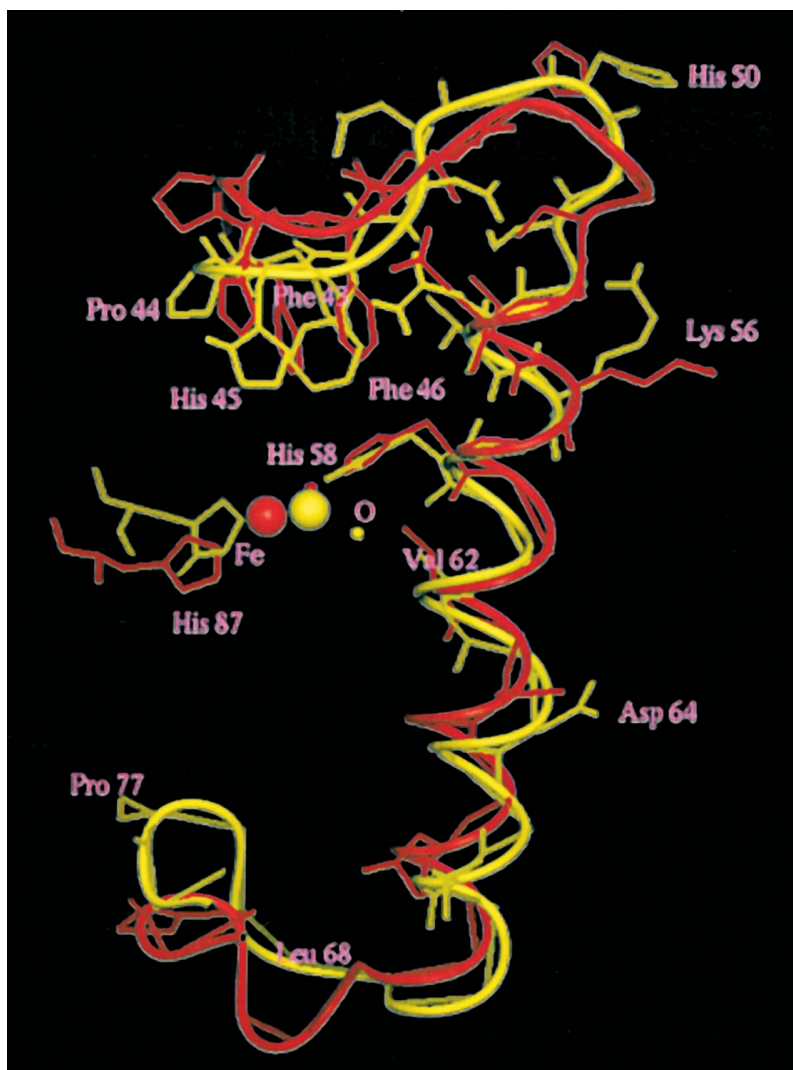
(Fig. 7), and changes in dihedral angles before the transition in both the G and H helices (Fig. 8). The $\alpha_1\beta_1$ interface has also been shown to play a role in producing the different rates of autoxidation found for the two types of chains. Thus, for isolated α- or β-chains (Tsuruga et al., 1998), the mechanism of autoxidation is similar, with similar rates for the two types of chains. However, low concentrations of hemoglobin corresponding to appreciable dissociation into $\alpha\beta$ dimers has the same chain heterogeneity found for tetramers (Tsuruga and Shikama, 1997).

An analogous linkage between the coordination with Fe and motion at the subunit interface has been detected by resonance Raman (Rousseau et al., 1993) in a study on deoxy dimeric hemoglobin (HbI) with Phe[97] at the subunit interface exhibiting perturbed motion due to ligand binding. However, in HbI the two hemes are in direct contact, and although the perturbations in the interface are the result of ligand binding, they are not necessary for communication between hemes.

The results of the molecular dynamics simulation are consistent with previous electron paramagnetic resonance studies on valency hybrids (Levy et al., 1992), which have provided experimental evidence for the transmission of conformational information from the distal heme pocket across the $\alpha_1\beta_1$ interface. It was found that replacing O_2 with CO on the reduced chains caused a perturbation in the distal heme pocket of the oxidized chains. By comparing the results with different valency hybrids, it was shown that this phenomenon involved transmission across the $\alpha_1\beta_1$ interface.

The EPR results from valency hybrids (Levy et al., 1992) and the autoxidation results (Tsuruga and Shikama, 1997) indicate that perturbations in the distal heme pocket involve the $\alpha_1\beta_1$ interface, despite the negligible structural changes found at this interface by static x-ray crystallography (Baldwin and Chothia, 1979; Fermi, 1975; Perutz, 1970; TenEyck and Arnone, 1976).

One resolution of this paradox has been proposed in a recent paper (Nichols et al., 1997). They have analyzed the structure of the $\alpha_1\beta_1$ interface of both oxyhemoglobin and deoxyhemoglobin in terms of rigid domains. In their analysis, 44–51% of the dimer that spans the interface is con-

sidered a rigid core. Although no structural deformations take place at the interface, intradimer allosteric coupling between hemes can take place by displacement of the whole rigid core when one of the heme pockets is perturbed, i.e., by formation of a bis-histidine complex.

In this analysis they have utilized the rigid x-ray structures. The molecular dynamics simulations, however, indicate that structural perturbations associated with the distal histidine transition are found to take place in the region of the interface. These perturbations are shown in Fig. 10, which compares three snapshots of the interface before the transition (50 ps), at the transition (60 ps), and after the transition (70 ps). Ribbon structures drawn connecting the C_α atoms (Fig. 10 A) reveal the structural changes involving the G and H helices in the interface. It is remarkable how the backbone of the G helix changes during the transition with the rearrangement enhanced after the transition. Another feature, namely the approach of the G and H helices in the α-subunit and the GH loop of the β-subunit toward each other, is clearly seen during the transition. The GH loop of the β-subunit moves back to its original position after the transition (70 ps), but the close contact between the G and H helices of the α-subunit is maintained and, in fact, increases even after the transition. The surface enclosed by the van der Waals radii of all of the atoms in the G and H helices of both the α- and β-subunits is shown in Fig. 10 B. The increased packing of the G and H helices at the interface is clearly seen both during and after the transition. This increased packing is also seen in the intersubunit DCCM (Fig. 5, A–C), where the contact region involving the G and H helices is strengthened during the transition with further amplification and spreading after the transition.

The perturbations in the distal pocket associated with bis-histidine complex formation are thus propagated to the interface compressing it. The interface acts like a buffer to relax the stearic strain and, thereby, stabilizes the biliganded complex. This role of the interface explains why the simulations with isolated subunits and dimer with frozen interface do not result in formation of the bis-histidine complex.

Propagation of conformational perturbations between the hemes and the interface

An explanation of the propagation of perturbations requires the availability of structural probes throughout the molecule. Although in principle high-resolution nuclear magnetic resonance can experimentally provide such information, it is still very difficult to obtain the necessary resolution. In this respect the strength of molecular dynamic simulations is the ability to obtain detailed information regarding each amino acid residue at any point in the simulation. Thus values for the dihedral angles actually provide the detailed configuration of every amino acid at each time point.

The time course for the changes in dihedral angles for residues within 5 Å of the distal histidine (Fig. 8) indicates

that most of the residues for which the dihedral angles change involve two regions of the molecule: 1) the CD loop lower E helix region of the α-chain and 2) the G helix and GH loop of the β-chain. These changes, some of which occur even before 30 ps, produce significant molecular rearrangements. The perturbations associated with the altered dihedral angles in the E helix and the CD loop of the α-chain are shown in Fig. 9. As shown in Fig. 11 for the α-chain G helix, the the altered dihedral angles of Phe[98](G5) dramatically alter the orientation of the phenylalanine side chain relative to the helix. Combining these data with the results obtained from RMS fluctuations, rupturing hydrogen bonds, changes in electrostatic interactions, and the DCCM (both intrasubunit and intersubunit), it is possible to begin to understand the propagation of conformational information through the $\alpha\beta$ dimer.

The intrasubunit DCCM (Fig. 4) indicates that correlated motion involving the lower E helix and the CD loop with the B helix in the interface is present initially in the α-chain but is appreciably strengthened during and after the transition. The altered dihedral angles in the CD loop and the lower E helix (Figs. 8 and 9) seem to be involved in the transmission of conformational information between the E helix and the B helix. The rearrangements in this region of the molecule are also indicated by the appreciable increase in the RMS fluctuations involving the CD loop and the lower E helix during and after the transition (Fig. 2, a and b). The rearrangements, which facilitate the approach of the distal histidine to the iron, appear to produce a stress on the E helix, which results in the rupturing of two hydrogen bonds in this region of the E helix (Lys[61]-Ala[65] at 55 ps and His[58]-Val[62] at 61 ps). The bend in the E helix after the transition can actually be visualized in Fig. 9. It is the lower E helix that approaches the heme, as seen in the more negative (attractive) electrostatic interactions of residues E5, E10, and E11 with the heme (Fig. 7). As the lower E helix undergoes increased correlated motion with the B helix in the interface during and after the transition, the upper E helix has increased positive correlated motion with the A helix extending away from the interface.

The altered dihedral angles involving the G and GH loop of the β-chain residues Leu[106](G8), Arg[116](G18), Lys[120](GH3), and Glu[125](GH8) before the transition suggest that the improved interface coupling in this region is initiated in part by changes in the G-GH segment of the β-chain. These changes appear to be associated with increased correlated motion between the α-chain B helix and the β-chain G-GH-H segment (Fig. 5, A and B). This section of the β-chain also undergoes increased RMS fluctuations (Fig. 2, c and d). These changes in the β-chain also coincide with more extensive coupled motion with the α-chain G helix (Fig. 5, A and B).

During the transition this improved packing at the interface also produces the ruptured hydrogen bonds in the beginning of the α-chain G helix located adjacent to the region of the G helix involved in contact with the β-chain G and H helices (Fig. 3). Together with this rearrangement at
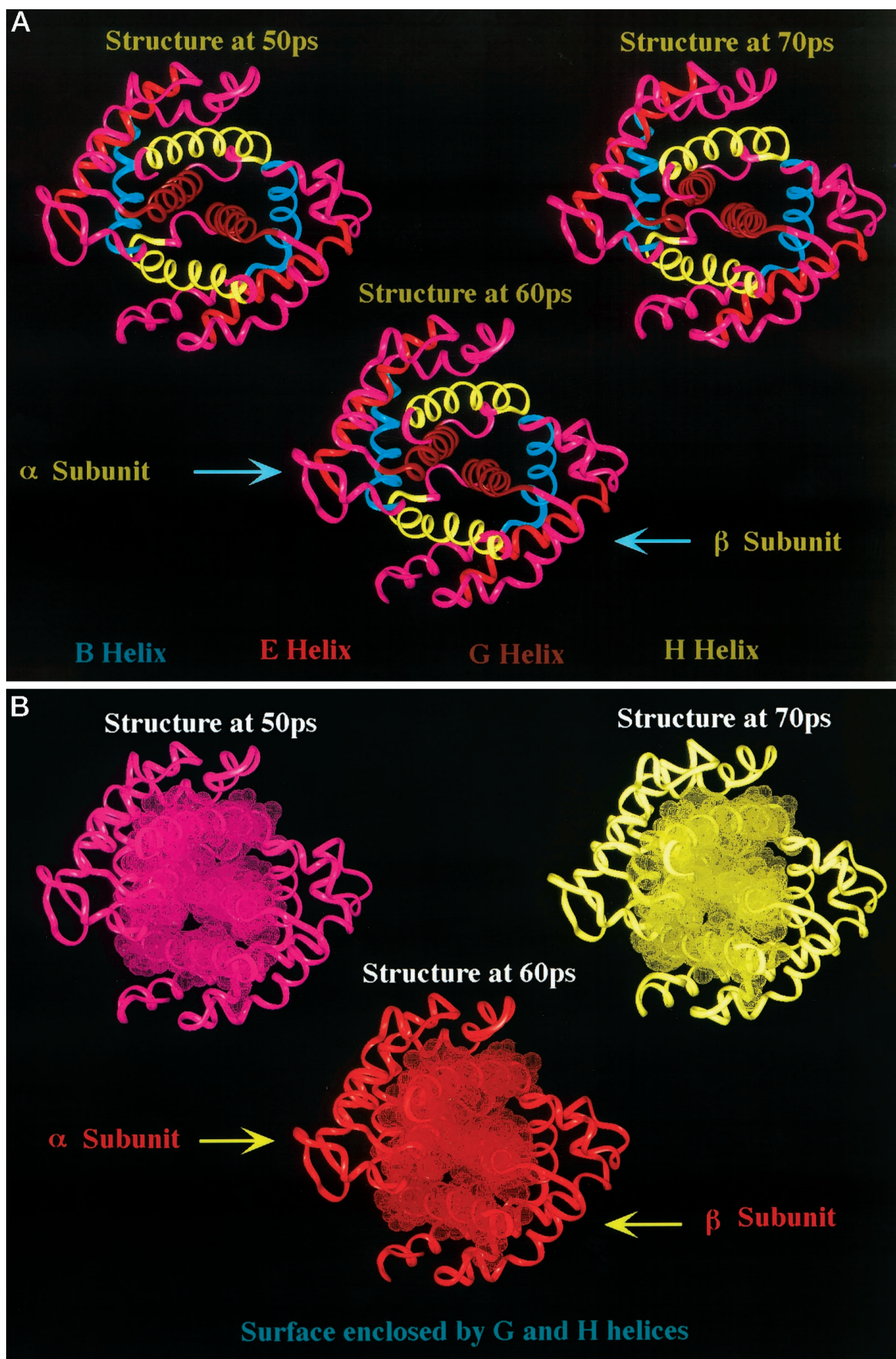
FIGURE 10 Comparison of the structure of the $\alpha\beta$ dimer before the bis-histidine transition (depicted by the 50-ps snapshot), during the bis-histidine transition (depicted by the 60-ps snapshot), and after the bis-histidine transition (depicted by the 70-ps snapshot). (a) The ribbon diagram of the C_α trace. (b) The C_α trace, showing the surface enclosed by the G and H helices.

FIGURE 11 Changes in the configuration of the side chains of the α-chain G-helix before the bis-histidine transition (depicted by the 50-ps snapshot), during the bis-histidine transition (depicted by the 60-ps snapshot), and after the bis-histidine transition (depicted by the 70-ps snapshot). Phenylalanine for residue G5 is depicted by space-filling models to show changes in the orientation of the phenylalanine ring.
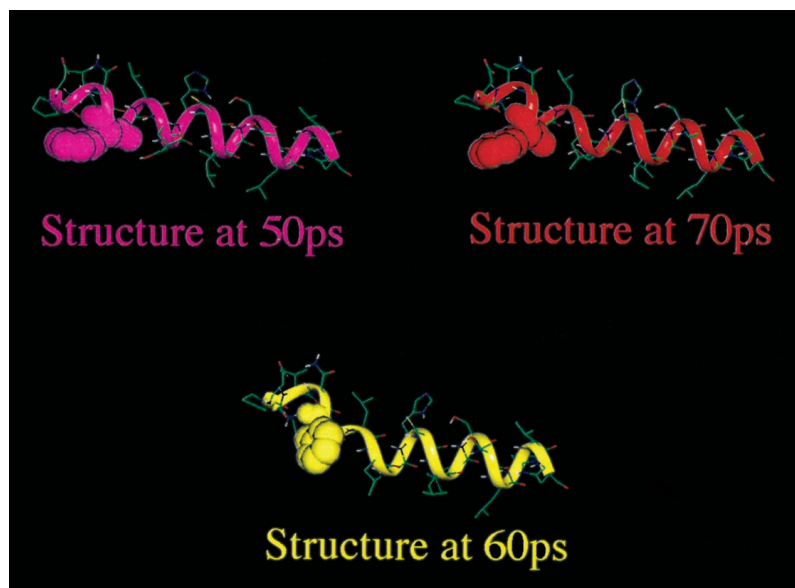
the interface (Fig. 10), altered electrostatic interactions (Fig. 7) and altered dihedral angles (Figs. 8 and 11) involving the α-chain G helix are produced. These interactions actually weaken the correlated motions in the contact region involving the β-chain B helix. Thus, after the transition when the N_ϵ of the distal histidine has moved closer to the iron, the correlated motion involving the α-chain B helix and the β-chain decrease (Fig. 5 C), even though the correlated motion involving the upper G helix and the G-GH-H region of the β-chain is further amplified.

Differences between the α-chain and the β-chain

The finding that a distal histidine iron bond is formed after 61 ps in the α-chain, but that no distal histidine bond is formed in the β-chain even after 100 ps, indicates a dramatic difference between both chains. The molecular dynamics simulation provides insight into the basis for these differences. The intrasubunit DCCM for the α-chain (Fig. 4, A–C) and the β-chain (Fig. 4, D–F) indicate distinct differences between the two types of chains that can influence the propagation of conformational perturbations between the distal heme pocket and the interface. Thus the correlated motion between the B helix and both the E helix and G helices are initially missing in the β-chain, and even after the transition they are much weaker in the β chain than in the α-chain. It has been suggested above that the propagation of conformational perturbations via this pathway are initiated by changes in the CD loop. However, because of the much longer D helix in the β-chain, the perturbations in the CD loop will not have the same affect on the interactions between the E helix and the B helix. An additional factor that mitigates against perturbations being propagated between the distal heme pocket to the interface via the B helix is the weakening of the coupled motion between the β-chain B helix and the G-GH-H region of the α-chain. This region

of the interface (Fig. 3) actually undergoes weakened coupled motion (Fig. 5, A–C) during and after the transition.

Instead, transmission between the interface and the β-chain distal pocket is probably associated with the coupled motion between the H helix and the F helix (Fig. 4, D–F). This coupled motion, which is very weak in the α-chain before the transition, is much more extensive in the β-chain and is further strengthened during and after the transition. This coupling in the α-chain may require the lengthening of the Fe-N_ϵ proximal histidine bond, which takes place as a result of the interaction of the distal histidine with the iron. However, in the β-chain this coupled motion occurs independently of the interaction of the distal histidine with the iron. The correlated motion in this region of the β-chain (Fig. 4, D–E) includes, and is actually dominated by, the EF loop. The EF loop and the upper E helix of the β-chain are very flexible before the transition (Fig. 2, c and d) and undergo an appreciable decrease in B factors during and after the transition. These results suggest that the communication between the interface and the distal pocket of the β-chain proceeds via the EF loop.

Fig. 5 C actually indicates positive correlated motion between the E helices of the α- and β-chains. This correlated motion is actually consistent with the EPR results, which indicate that in valency hybrids (Levy et al., 1992) conformational coupling is transmitted between the distal heme pockets of the two chains via the $\alpha_1\beta_1$ interface. According to the analysis of our molecular dynamics simulations, this interaction is understood in terms of distinct pathways in the α- and β-chains linking the heme pocket with the interface. However, only in the α-chain, as a result of the coupled motion between the E helix and the B helix, is the distal histidine brought into the proper configuration to bond with the iron. The pathway via the EF loop does not facilitate this rearrangement. This explains why no distal histidine bond was formed in the β-chain during a 100-ps

simulation. Movement of the N_ϵ of the distal histidine closer to the iron before initiating the simulation was shown (unpublished results) to be required for the formation of a distal histidine bond within 100 ps in the β-chain.

CONCLUSION

The molecular dynamics simulations reported in this paper have been limited to an $\alpha\beta$ dimer without the addition of water. The relevance of these results to hemoglobin is supported, however, by the finding that the simulations were able to mimic experimental results. The experimental results include the temperature-dependent formation of a bond between the distal histidine and the iron (Levy and Rifkind, 1985; Levy et al., 1990), as well as the involvement of the $\alpha_1\beta_1$ interface in distal pocket perturbations (Levy et al., 1992), which can actually be propagated between subunits. The simulations, however, extend our understanding of these molecular processes predicting certain rearrangements that thus far have not been elucidated by experimental results. Thus it is shown that the interaction of the distal histidine with the iron takes place preferentially in the α-chain. It is also shown that the rearrangements necessary to bring the histidine closer to the iron involve alterations primarily in the CD loop and at the interface. Communication to the β-chain distal pocket is related to the flexibility in the EF loop. The predictions of this study can eventually be tested by the preparation of hemoglobins with altered amino acid sequences.

We have used an $\alpha\beta$ dimer for our molecular dynamics simulation, to focus on the perturbations at the $\alpha_1\beta_1$ interface and the role of this interface in the propagation of interactions between chains. The processes found to take place in our simulations may be relevant, however, to the propagation of conformational changes across the subunit interfaces in a tetramer. The G helix, which has been shown to undergo major changes during our simulation (Figs. 10 and 11), extends from the $\alpha_1\beta_2$ interface, which includes Asp^{94}(G1), Pro^{95}(G2), and Val^{96}(G3), to the $\alpha_1\beta_1$ interface, which includes His^{103}(G10), Cys^{104}(G11), Leu^{106}(G13), Ser^{107}(G14), and Val^{111}(G18). Many of the perturbations found in our analysis involve the residues between Val^{96} and His^{103}, which link the segments of the G helix associated with the two types of interfaces. The compaction found in our analysis will therefore also modulate the rearrangements taking place in the $\alpha_1\beta_2$ interface during ligand binding. This prediction suggests a mechanism whereby the dynamic fluctuations transmitted across the $\alpha_1\beta_1$ interface modulate the quaternary transition primarily involving the $\alpha_1\beta_2$ interfaces. In this respect it is interesting to note that changes in fluctuations are found in the first few G helix residues, which link both interfaces, when comparing the T and R states of hemoglobin (Baldwin and Chothia, 1979; Nichols et al., 1995).

REFERENCES

Ackers, G. K., M. L. Doyle, D. Myers, and M. A. Daugherty. 1992. Molecular code for cooperativity in hemoglobin. *Science.* 255:54–63.

Anderson, L. 1973. Intermediate structure of normal human haemoglobin: methaemoglobin in the deoxy quaternary conformation. *J. Mol. Biol.* 79:495–506.

Anderson, L. 1975. Structures of deoxy and carbonmonoxy haemoglobin Kansas in the deoxy quaternary conformation. *J. Mol. Biol.* 94:33–49.

Arata, Y. 1995. Effect of the tertiary structure alteration by ligation on the interface contacts between subunits of hemoglobin. *Biochim. Biophys. Acta.* 1247:24–34.

Arata, Y., Y. Seno, and J. Otsuka. 1988. A study on the quaternary structure change of hemoglobin in the ligation process. *Biochim. Biophys. Acta.* 956:243–255.

Atha, D. H., and A. Riggs. 1976. Tetramer-dimer dissociation in homoglobin and the Bohr effect. *J. Biol. Chem.* 251:5537–5543.

Balagopalakrishna, C., P. T. Manoharan, O. O. Abugo, and J. M. Rifkind. 1996. Production of superoxide from hemoglobin-bound oxygen under hypoxic conditions. *Biochemistry.* 35:6393–6398.

Baldwin, J., and C. Chothia. 1979. Haemoglobin: the structural changes related to ligand binding and its allosteric mechanism. *J. Mol. Biol.* 129:175–220.

Barksdale, A. D., and A. Rosenberg. 1978. Thermodynamic characterization of subunit association in liganded ferrohemoglobin. The temperature pH and anion dependence of the carboxyhemoglobin A dimer-tetramer equilibrium. *J. Biol. Chem.* 253:4881–4885.

Bjorling, S. C., R. A. Goldbeck, S. J. Paquette, S. J. Milder, and D. S. Kliger. 1996. Allosteric intermediates in hemoglobin. 1. Nanosecond time-resolved circular dichroism spectroscopy. *Biochemistry.* 35:8619–8627.

Brooks, B. R., R. E. Bruccoleri, B. D. Olafson, D. J. States, S. Swaminathan, and M. Karplus. 1983. CHARMM: a program for macromolecular energy, minimization, and dynamics calculations. *J. Comp. Chem.* 4:87–217.

Bucci, E., C. Fronticelli, Z. Gryczynski, A. Razynska, and J. H. Collins. 1993. Effect of intramolecular cross-links on the enthalpy and quaternary structure of the intermediates of oxygenation of human hemoglobin. *Biochemistry.* 32:3519–3526.

Carlson, M. L., R. M. Regan, and Q. H. Gibson. 1996. Distal cavity fluctuations in myoglobin: protein motion and ligand diffusion. *Biochemistry.* 35:1125–1136.

Doyle, M. L., and G. K. Ackers. 1992. Cooperative oxygen binding, subunit assembly, and sulfhydryl reaction kinetics of the eight cyanomet intermediate ligation states of human hemoglobin. *Biochemistry.* 31:11182–11195.

Fermi, G. 1975. Three-dimensional Fourier synthesis of human deoxyhaemoglobin at 2–5 Å resolution: refinement of the atomic model. *J. Mol. Biol.* 97:237–256.

Gelin, B. R., A. W.-M. Lee, and M. Karplus. 1983. Hemoglobin tertiary structural change on ligand binding. Its role in the co-operative mechanism. *J. Mol. Biol.* 171:489–559.

Guenot, J., and P. A. Kollman. 1993. Conformational and energetic effects of truncating nonbonded interactions in an aqueous protein dynamics simulation. *J. Comp. Chem.* 14:295–311.

Harvey, S. 1989. Treatment of electrostatic effects in macromolecular modeling. *Proteins.* 5:78–92.

Ho, C. 1992. Proton nuclear magnetic resonance studies on hemoglobin: cooperative interactions and partially ligated intermediates. *Adv. Protein Chem.* 43:153–312.

Holt, J. M., and G. K. Ackers. 1995. The pathway of allosteric control as revealed by hemoglobin intermediate states. *FASEB J.* 9:210–218.

Huang, Y., and G. K. Ackers. 1995. Enthalpic and entropic components of cooperativity for the partially ligated intermediates of hemoglobin support a "symmetry rule" mechanism. *Biochemistry.* 34:6316–6327.

Ichiye, T., and M. Karplus. 1991. Collective motions in proteins: a covariance analysis of atomic fluctuations in molecular dynamics and normal mode simulations. *Proteins.* 11:205–217.

Kellett, G. L., and H. K. Schachman. 1971. Dissociation of hemoglobin into subunits. Monomer formation and the influence of ligands. *J. Mol. Biol.* 59:387–399.

Komeiji, Y., M. Uebayasi, and I. Yamato. 1994. Molecular dynamics simulations of trp apo- and holorepressors: domain structure and ligand-protein interaction. *Proteins.* 20:248–258.

Kwiatkowski, L. D., A. De-Yound, and R. W. Noble. 1994. Isolation and stability of partially oxidized intermediates of carp hemoglobin: kinetics of CO binding to the mono- and triferric species. *Biochemistry.* 1994: 5884–5893.

Ladner, R. C., E. J. Heidner, and M. F. Perutz. 1977. The structure of horse methaemoglobin at 2.0 Å resolution. *J. Mol. Biol.* 114:385–414.

Lee, F. S., and A. Warshel. 1992. A local reaction field method for fast evaluation of long-range electrostatic interactions in molecular simulations. *J. Chem. Phys.* 97:3100–3107.

Levy, A., P. Kuppusamy, and J. M. Rifkind. 1990. Multiple heme pocket subconformations of methemoglobin associated with distal histidine interactions. *Biochemistry.* 29:9311–9316 .

Levy, A., and J. M. Rifkind. 1985. Low-temperature formation of a distal histidine complex in hemoglobin: a probe for heme pocket flexibility. *Biochemistry.* 24:6050–6054.

Levy, A., V. S. Sharma, L. Zhang, and J. M. Rifkind. 1992. A new mode for heme-heme interactions in hemoglobin associated with distal perturbations. *Biophys. J.* 61:750–755.

Loncharich, R. J., and B. R. Brooks. 1989. The effects of truncating long-range forces on protein dynamics. *Proteins.* 6:32–45.

Lumry, R. 1994. A new paradigm for protein research. *In* Protein-Solvent Interactions. R. Gregory, editor. Marcel Dekker, New York.

Lumry, R., and R. Gregory. 1989. Dynamical factors in protein-protein association. *J. Mol. Liq.* 42:113–144.

Matthew, J. B. 1985. Electrostatic effects in proteins. *Annu. Rev. Biophys. Chem.* 14:387–417.

Mehler, E. L., and T. Solmajer. 1991. Electrostatic effects in proteins: comparison of dielectric and charge models. *Protein Eng.* 4:903–910.

Moffat, K., J. F. Deatherage, and D. W. Seybert. 1979. A structural model for the kinetic behavior of hemoglobin. *Science.* 206:1035–1042.

Nichols, W. L., G. D. Rose, L. F. Ten Eyck, and B. H. Zimm. 1995. Rigid domains in proteins: an algorithmic approach to their identification. *Proteins.* 23:38–48.

Nichols, W. L., B. H. Zimm, and L. F. Ten Eyck. 1997. Conformation-invariant structures of the $\alpha_1\beta_1$ human hemoglobin dimer. *J. Mol. Biol.* 270:598–615.

Perrella, M., N. Davids, and L. Rossi-Bernardi. 1992. The association reaction between hemoglobin and carbon monoxide as studied by the isolation of the intermediates. Implications on the mechanism of cooperativity. *J. Biol. Chem.* 267:8744–8751.

Perutz, M. F. 1970. Stereochemistry of cooperative effects in haemoglobin. *Nature.* 228:726–739.

Perutz, M. F. 1989. Myoglobin and hemoglobin: role of distal residues in reactions with heme ligands. *Trends Biochem. Sci. Lett.* 14:42–44.

Rifkind, J. M. 1988. Hemoglobin. *In* Advances in Inorganic Biochemistry, Vol. 7. G. L. Eichhorn and L. G. Marzilli, editors. Elsevier/North Holland, New York. 155–244.

Rosemeyer, M. A., and E. R. Huehns. 1967. On the mechanism of the dissociation of haemoglobin. *J. Mol. Biol.* 25:253–273.

Rousseau, D. L., S. Song, J. M. Friedman, A. Boffi, and E. Chiancone. 1993. Heme-heme interactions in a homodimeric cooperative hemoglobin—evidence from transient Raman scattering. *J. Biol. Chem.* 268: 5719–5723.

Sharp, K. A., and B. Honig. 1990. Electrostatic interactions in macromolecules: theory and applications. *Annu. Rev. Biophys. Chem.* 19:301–332.

Solmajer, T., and E. L. Mehler. 1991. Electrostatic screening in molecular dynamics simulations. *Protein Eng.* 4:911–917.

Steinbach, P. J., and B. R. Brooks. 1994. New spherical-cutoff methods for long-range forces in macromolecular simulation. *J. Comput. Chem.* 15:667–683.

Stote, R. H., D. J. States, and M. Karplus. 1991. On the treatment of electrostatic interactions in biomolecular simulation. *J. Chim. Phys.* 88:2419–2433.

Swaminathan, S., W. E. Harte, Jr., and D. L. Beveridge. 1991. Investigation of domain structure in proteins via molecular dynamics simulation: application to HIV-1 protease dimer. *J. Am. Chem. Soc.* 113:2717–2721.

TenEyck, L. F., and A. Arnone. 1976. Three-dimensional Fourier synthesis of human deoxyhemoglobin at 2–5 Å resolution. I. X-ray analysis. *J. Mol. Biol.* 100:3–11.

Tian, W. D., J. T. Sage, and P. M. Champion. 1993. Investigations of ligand association and dissociation rates in the "open" and "closed" states of myoglobin. *J. Mol. Biol.* 233:155–166.

Tsuruga, M., A. Matsuoka, A. Hachimori, Y. Sugawara, and K. Shikama. 1998. The molecular mechanism of autoxidation for human oxyhemoglobin. *J. Biol. Chem.* 273:8607–8615.

Tsuruga, M., and K. Shikama. 1997. Biphasic nature in the autoxidation reaction of human oxyhemoglobin. *Biochim. Biophys. Acta.* 1337: 96–104.

van Gunsteren, W. F., and H. J. Berendsen. 1984. Computer simulation as a tool for tracing the conformational differences between proteins in solution and in the crystalline state. *J. Mol. Biol.* 176:559–564.